AAS 17-826

STATIONKEEPING AND TRANSFER TRAJECTORY DESIGN FOR SPACECRAFT IN CISLUNAR SPACE

Diane C. Davis,[*] Sean M. Phillips,[†] Kathleen C. Howell,[‡] Srianish Vutukuri,[§] and Brian P. McCarthy[§]

NASA's Deep Space Gateway (DSG) will serve as a staging platform for human missions beyond the Earth-Moon system and a proving ground for inhabited deep space flight. With a Near Rectilinear Halo Orbit (NRHO) serving as its primary long-term orbit, the DSG is planned to execute excursions to other destinations in cislunar space. The current study explores the details of generating NRHOs in high-fidelity force models. It then investigates the cost of stationkeeping the primary and destination orbits. Finally, Poincaré maps are employed in a visual design process for preliminary transfer design between candidate orbits in cislunar space.

INTRODUCTION

NASA's recently announced Deep Space Gateway[1] (DSG) is planned to take advantage of the complex multibody dynamical region in cislunar space. Starting with the Exploration series of missions in the mid-2020s, NASA plans to assemble the DSG in a Near Rectilinear Halo Orbit (NRHO) near the Moon.[2] A member of the halo family of orbits, the candidate NRHO is characterized by a period of approximately one week, nearly polar passages of the Moon at perilune, and behavior that exhibits nearly stable characteristics. By the end of the 2020s, NASA plans to exercise the capability to transfer the gateway spacecraft from the NRHO to other orbits in cislunar space as a demonstration and shakedown of deep space flight capabilities. Candidate destinations include other members of the L_1 and L_2 halo families as well as butterfly orbits, among other options.

These candidate destination orbits exist within periodic orbit families in the dynamical environment described by the Circular Restricted 3-Body Problem (CR3BP)[3] and persist as quasi-periodic trajectories when transitioned to higher-fidelity models. Multiple methods exist for transitioning an orbit from a periodic solution in the CR3BP to a quasi-periodic orbit in an ephemeris model;[4,5,6] specific implementations affect the resulting orbit. This study discusses the families of orbits under investigation and their properties viewed in the CR3BP, and then explores the transition into higher-fidelity models.

A second topic of investigation is stationkeeping of the spacecraft in selected primary and destination orbits. The orbits under consideration have different stability properties and require different strategies for long-term orbit maintenance. Multiple strategies for stationkeeping libration point orbits have been previously investigated; overviews of various methods appear in Folta et al.[7] and Guzzetti et al.[8] Halo orbit stationkeeping has been investigated across the L_1 and L_2 families in the CR3BP by Folta et al.,[9,10] and

[*] Principal Systems Engineer, a.i. solutions, Inc., 2224 Bay Area Blvd, Houston TX 77058, diane.davis@ai-solutions.com.
[†] Principal Software Engineer, a.i. solutions, Inc., 4500 Forbes Blvd., Lanham MD 20706, sean.phillips@ai-solutions.com.
[‡‡] Hsu Lo Distinguished Professor, School of Aeronautics and Astronautics, Purdue University, Armstrong Hall of Engineering, 701 W. Stadium Ave., West Lafayette, IN 47907-2045, howell@purdue.edu. Fellow AAS; Fellow AIAA.
[§] Graduate Student, School of Aeronautics and Astronautics, Purdue University, Armstrong Hall of Engineering, 701 W. Stadium Ave., West Lafayette, IN 47907-2045, svutukur@purdue.edu and mccart71@purdue.edu.

methods have been proven in flight for specific halos in the Sun-Earth system[11] and the Earth-Moon system.[12] Stationkeeping of the L_2 southern NRHOs is studied by Guzzetti et al.[8] and Davis et al.,[13] who propose low-cost strategies for long-term orbit maintenance of crewed and uncrewed spacecraft. The current study builds on previous efforts, exploring stationkeeping of the L_1 NRHOs as well as looking broadly at stationkeeping across the L_1 and L_2 Halo families. Then, stationkeeping of the southern L_2 butterfly family is investigated.

A third topic of investigation is the design of transfer trajectories between a starting NRHO and various destination orbits. Transfers between multibody orbits have been investigated by many researchers.[14,15,16] The current study employs periapsis Poincaré maps[17,18] for preliminary transfer design. Maps are overlaid to generate initial transfer arcs that are then corrected into continuous trajectories in the CR3BP. NRHO to unstable halo orbit transfer orbits are explored, and two families of NRHO to butterfly orbit transfers are generated.

DYNAMICAL MODELS

In this investigation, two dynamical models are employed. The CR3BP provides the framework for generation and analysis of libration point orbit families and preliminary transfer design, and an n-body ephemeris model simulates higher-fidelity mission applications.

The CR3BP describes the motion of a massless spacecraft affected by two primary gravitational bodies such as the Earth and the Moon. The model assumes that the two primary bodies are point masses orbiting their center of mass in circular orbits. The spacecraft moves freely under the influence of the two primaries, and its motion is described relative to a rotating reference frame. No closed-form solution exists to the CR3BP equations of motion, but five equilibrium solutions, the libration points, are denoted L_1 through L_5. Stable and unstable periodic orbit families are found in the vicinity of the libration points. A single integral of the motion exists in the CR3BP. The Jacobi integral, or Jacobi constant, *J*, is written

$$J = 2U^* - v^2 \tag{1}$$

where *v* is the velocity magnitude of the spacecraft relative to the rotating frame and U^* is the pseudo-potential function.

A higher fidelity model incorporates N-body equations of motion and NAIF planetary ephemerides. A Moon-centered J2000 inertial coordinate frame is selected for integration, with point-mass perturbations by the Sun and Earth included. In some simulations, the Moon's gravity is modeled using the GRAIL (GRGM660PRIM) model truncated to degree and order 8.

EARTH-MOON HALO AND BUTTERFLY ORBITS

Many families of periodic and quasi-periodic orbits exist in the vicinity of the five libration points in the CR3BP.[19] The halo orbits[20] are well-known families near the collinear libration points L_1, L_2, and L_3. In the Earth-Moon system, the L_1 and L_2 families bifurcate from planar Lyapunov orbits around the libration points and evolve out of plane until they approach the Moon. Representative halos appear in Figure 1. A portion of the L_1 halo family appears in Figure 1a. The L_1 family extends from the planar Lyapunov orbit around L_1 and grows out of plane until the perilune radii are well within the Moon's radius. Since orbits that intersect with the Moon's surface are not applicable to the current study, only halos with perilune radius r_p > 1,800 km appear in Figure 1a. Note that as perilune radii approach the surface of the Moon, the apolune radii of the L_1 halos grow. This feature is in contrast to the L_2 halo orbits, appearing in Figure 1b. As the L_2 halo orbits approach the Moon, their apolune radii decrease. The orbital periods as a function of r_p appear in Figure 2a. The orbital periods of halos in the L_2 family range from 14.8 days near the libration point down to about 5.9 days near the lunar surface. The L_1 halos, in contrast, have a maximum orbital period of about 12 days at an r_p of ~43,500 km and a minimum period of about 7.5 days before the apolune radii begin to increase at r_p ~ 4,500 km; the periods of the L_1 halos increase as r_p values decrease further.

The NRHO[21] portions of the L_1 and L_2 halo families are defined by their stability properties. A stability index[22] is defined as a function of the maximum eigenvalue of the monodromy matrix, i.e., the state transition matrix (STM) associated with the halo orbit after precisely one revolution. The stability index is evaluated here as

$$\nu = \frac{1}{2}\left(\lambda_{max} + \frac{1}{\lambda_{max}}\right) \tag{2}$$

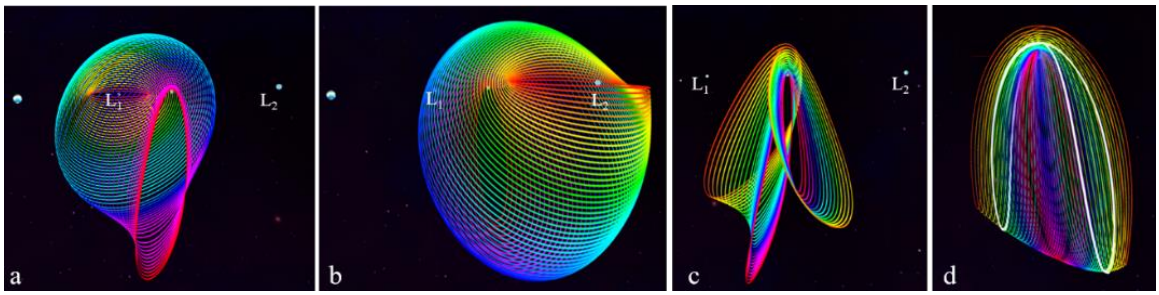

Figure 1. Periodic Orbits in the CR3BP: The portion of the L_1 southern halo family that remain above the Moon's surface at perilune (a); the L_2 southern halo family (b); L_1 and L_2 NRHOs (c); and the L_2 southern butterfly family (d).

A halo orbit characterized by a stability index equal to one is considered marginally stable from the linear analysis. A stability index greater than one corresponds to an unstable halo orbit; the higher the value of *ν*, the faster a perturbed halo orbit will tend to depart its nominal path. The stability index for the L_1 and L_2 halo families appears as a function of r_p in Figure 2a. The unstable, nearly planar halo orbits exist at the far right of the plot, characterized by high stability indices and large perilune distances. As the halo families evolve out of plane, their stability indices decrease as the orbits approach the Moon. At very small perilune radii, the halo orbits possess single-digit linear stability indices, as is apparent in the zoomed-in plot in Figure 2b. Above a perilune radius of around 17,350 km in the L_2 family and 19,500 km in the L_1 family, the stability indices rapidly increase. Within each halo family, the NRHOs can be defined as the subset of the halo families with bounded stability characteristics. The NRHO portions of the L_1 and L_2 southern halos appear in Figure 1c.

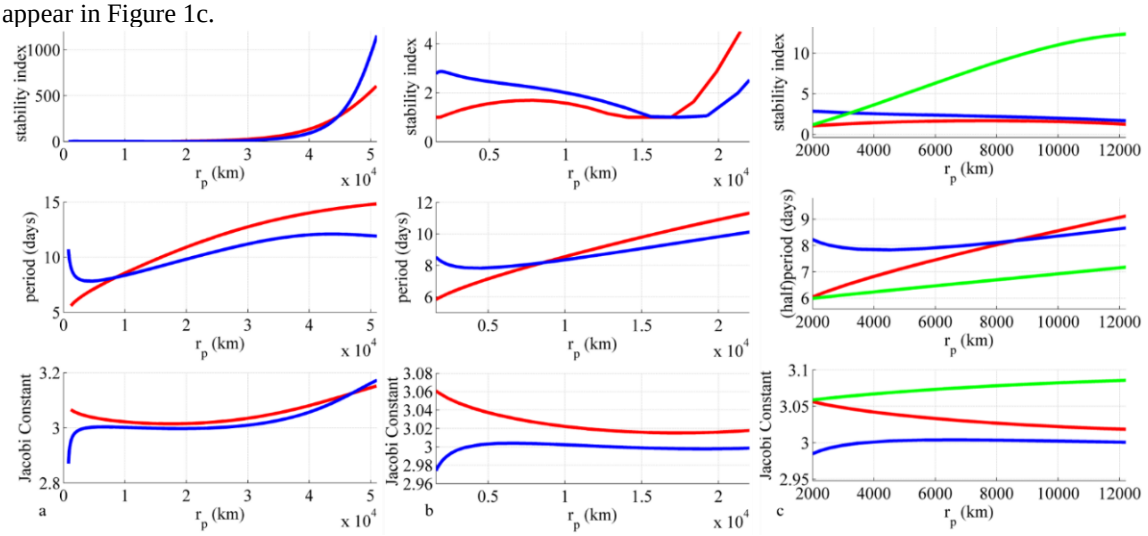

Figure 2. Family characteristics: Stability index, orbital period, and Jacobi constant across the L_1 (blue) and L_2 (red) halo families (a); Zoomed in on the NRHO regions (b); plotted with the L_2 butterfly family (green) (c).

The Jacobi constant *J* characterizes the energy of each orbit, with a lower value of *J* corresponding to a more energetic orbit. Like stability index and orbital period, the Jacobi constant associated with each halo orbit evolves along with perilune radius. In the L_2 family, *J* decreases as the halos evolve out of plane and then begins to increase again as r_p approaches the Moon. In the L_1 family, *J* decreases across the family with decreasing r_p and then dips quickly as apolune radii increase near the Moon. Jacobi constant across the L_1 and L_2 families appears in Figure 2.

Another periodic set of orbits in the CR3BP, the L_2 butterfly family bifurcates from one of the L_2 NRHOs.[22,23,24] The butterfly family is a recent topic of interest as a potential destination for DSG excursions. Like NRHOs, they demonstrate nearly stable behavior, and the southern family provides

coverage of the lunar south pole and favorable visibility to the Earth.[22] A set of L_2 southern butterfly orbits appears in Figure 1d. The orbital periods of the butterfly orbits are about double that of the NRHOs, since the butterflies wrap around the moon, making a loop on both the L_1 side and the L_2 side in a single period. The stability indices, the half-periods, and the Jacobi constants of a portion of the butterfly family (in green) are compared to the same quantities for the L_1 and L_2 halo families in Figure 2c. In each plot, the green line representing the butterfly family intersects with the red line corresponding to the L_2 halos at the point where the two families bifurcate. In general, the butterfly orbits are less stable, move more quickly around the Moon, and have a lower energy (higher value of *J*) than NRHOs at the same perilune radius.

TRANSITIONING TO A HIGHER-FIDELITY FORCE MODEL

The periodic orbits in the CR3BP exist as quasi-periodic motion in a higher-fidelity ephemeris force model. A halo trajectory can be constructed directly in a higher-fidelity force model. It is also common to compute the orbit within the context of the CR3BP where favorable characteristics are most apparent and constraints are straightforward to introduce. Methods of transitioning between models are well documented; two-level targeters,[4] differential correctors,[8] forward and forward-backward shooting methods, and receding horizon targeting[6] have all been successfully demonstrated, with no single algorithm emerging as a preferred method. In the current investigation, a differential correction method, a forward-backward shooting method, and two-level targeting are all employed.

Halo orbits

Across the halo families, the characteristics of the quasi-periodic orbits that result from transition to an ephemeris force model differ based on various parameters. For spaceflight applications, these characteristics can have significant effects on the stationkeeping costs, eclipsing properties, and other practical considerations. One characteristic of interest is the "tightness" of the orbit, or how close to periodic the trajectory appears. An apse angle[8] is defined to quantify the variation in the orbit from one revolution to the next. In the current study, apse angle is defined as the angle of the osculating line of apsides from the rotating z-axis at the time of perilune passage. The maximum apse angle of a quasi-periodic orbit is a measure of the variation in the orbit from a perfectly periodic halo. For a given method of transitioning the CR3BP periodic halo to an ephemeris model, the maximum apse angles of the resulting quasi-periodic orbits vary across the halo family. Fifteen members of the L_2 family appear in Figure 3. Qualitatively, it is apparent that the apse angles for small-r_p halos and large-r_p halos are small- these halo orbits are corrected into tight, nearly periodic orbits. In the middle of the family, a transition region is characterized by large variations in apse angles and less-periodic behavior.

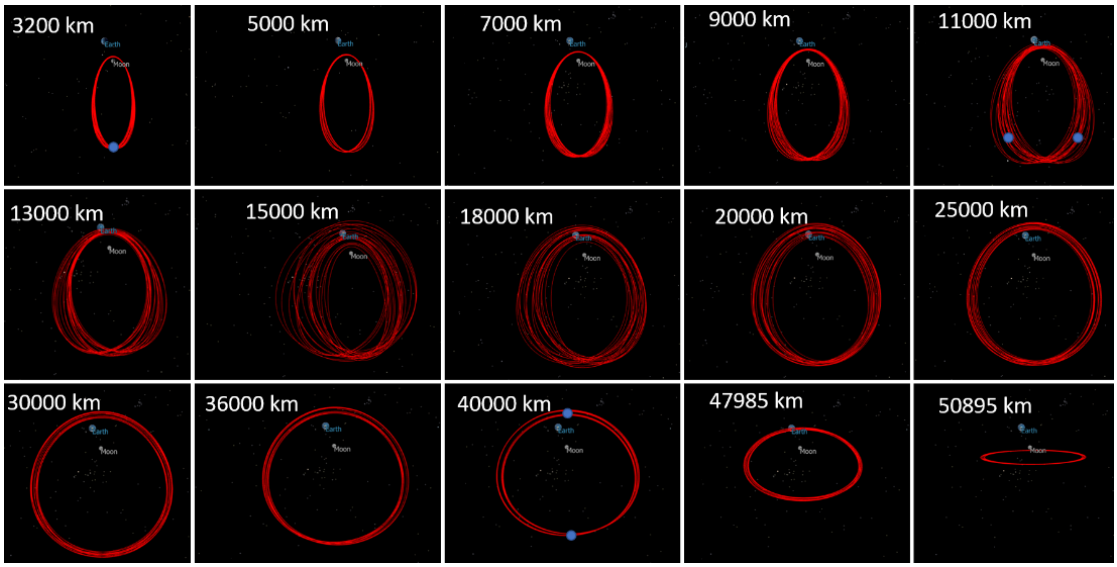

Figure 3. Fifteen members of the L_2 southern halo family with varying perilune radii transitioned from periodic CR3BP orbits to continuous quasi-periodic orbits in an ephemeris force model.

A similar set of orbits across the L_1 halo family appears in Figure 4. Again, tight, nearly periodic orbits are achieved at very large and very small values of perilune radius. In the center of the family, larger variations in apse angle are observed. Patterns can be observed in the variations in orbits, particularly in orbits in a near-resonance with the Moon. For example, repetitive behavior is present in the 18,000 km L_1 halo in the center of Figure 4. Repetitive behavior in halo orbits that possess large variations in apse angle is desirable for reasons including eclipse avoidance. Careful generation of a reference halo orbit can lead to distinct patterns in the resulting orbit that can be exploited to satisfy mission design objectives.

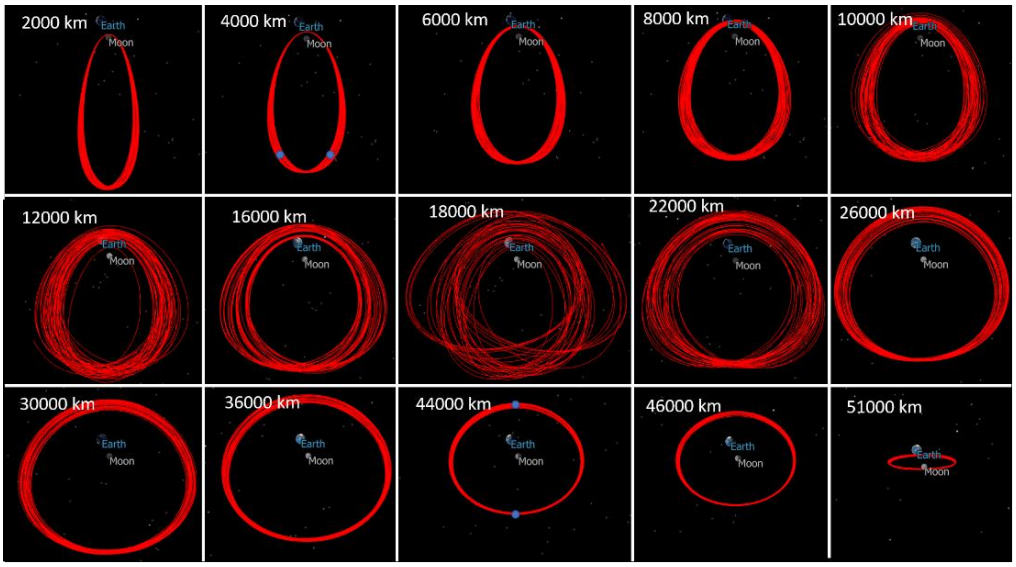

Figure 4. Fifteen members of the L_1 southern halo family with varying perilune radii transitioned from periodic CR3BP orbits to continuous quasi-periodic orbits in an ephemeris force model.

Node Phasing for Repeating Behavior

Halo orbits in a lunar synodic resonance are of interest due to their potential for eclipse avoidance.[6,8,24] L_2 NRHOs in 9:2 and 4:1 synodic resonances possess perilune radii of ~3,200 km and ~6,000 km respectively, and these orbits are easily transitioned into ordered references with small variations in apse angle in higher-fidelity force models. Also of interest is an L_2 NRHO in a 3:1 lunar synodic resonance. With a perilune radius of approximately 15,000 km and a period of 9.8 days, this orbit is marginally stable in a linear CR3BP analysis. Like the 4:1 synodic resonant NRHO, the 3:1 NRHO has the potential to allow a spacecraft to avoid eclipses by both the Earth and the Moon with proper orientation. However, the 3:1 NRHO lies in the transition region characterized by large variations in apse angle. With careful generation of a reference orbit in a higher-fidelity force model, particular characteristics and patterns can be maintained in the orbit.

When transitioning a periodic orbit from the CR3BP to a higher-fidelity model, it is typical to employ a stacking procedure in which the representative states for a simply symmetric halo from the CR3BP are stacked over multiple revolutions—one set on top of the other until the time interval over the sequentially stacked orbits roughly corresponds to the total duration for the mission. For instance, if twelve 3:1 synodic resonant NRHOs are stacked, the total time is 98 days. The originating point for the stacked trajectory is notable. Assume that the first point along the stacked trajectory is arbitrarily selected to be located on the *x*-*z* plane. The stacked trajectory is decomposed into sub arcs by distributing nodes along each orbit in the stack. The trajectory, comprised of multiple revolutions of the periodic orbit in the circular restricted model, is represented by a sequence of six-dimensional states at each of the nodes. Each state is associated with a time tag that reflects the time since the initial state along the path. A state in the CR3BP is non-dimensional, and each state is dimensionalized appropriately. Most significantly, perhaps, is the characteristic length, i.e., the Earth-Moon distance. To dimensionalize the state at each node, the instantaneous Earth-Moon distance at the associated epoch is employed. During the differential corrections process, position and velocity continuity is enforced across each node, and the state vectors are then

adjusted appropriately in the higher-fidelity ephemeris model to produce a continuous path. The time associated with the first node, located on the *x*-*z* plane, corresponds to a specific epoch.

Consider a set of 3:1 resonant NRHOs commencing during May 2023. On each day of the month, an identical set of stacked nodes representing twelve revolutions of the NRHO from the CR3BP is transitioned into the ephemeris model. A representative set of orbits appear in Figure 5 in the Earth-Moon rotating frame. A clear pattern of tightly (less spread) or loosely (more spread) converged trajectories is visible across the month. The pattern roughly repeats every 9 or 10 days corresponding to the period. The 3:1 resonance is clearly visible on the days of the month with more repeatable behavior.

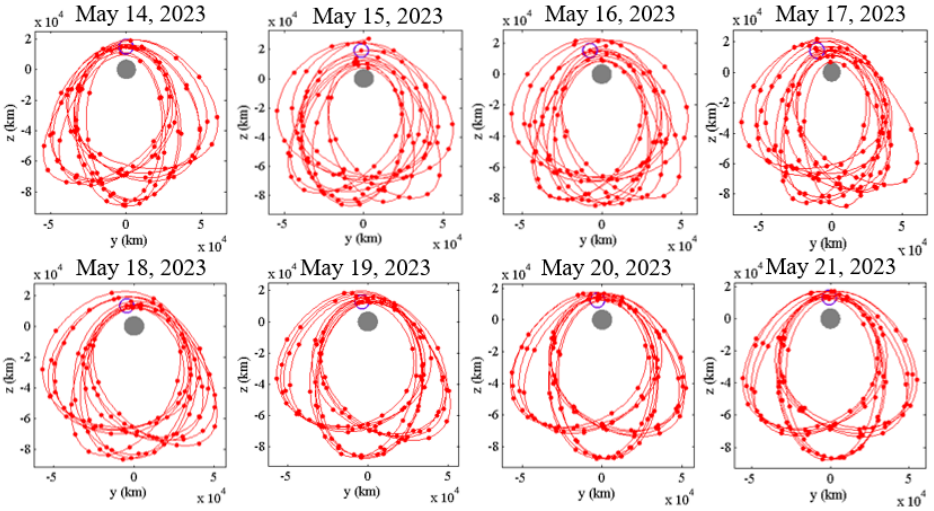

Figure 5. Eight sample 3:1 lunar synodic resonant NRHOs transitioned into a higher-fidelity force model using the same set of CR3BP patch points on different dates in May 2023.

To characterize the spread of the trajectory in the ephemeris model, the apse angle is employed. The apse angle for each revolution as evaluated in the CR3BP is zero since the orbit is strictly periodic and the line of apsides is aligned with the *z*-axis for every revolution. After transition to the ephemeris force model, the apse angle can vary widely for the 3:1 NRHOs. Additionally, perilune radius also varies, and as is apparent in Figure 5, r_p values have a larger range for the less well ordered NRHOs as compared to those with distinct patterns. Plots of the apse angle and Δr_p for two sample trajectories appear in Figure 6. The plots in Figure 6a correspond to the trajectory in Figure 5 that commences on May 16. This disorderly trajectory has a wide variation in r_p, but the 3:1 pattern remains present in the pattern of apse angle. The plots in Figure 6b represent the well-ordered NRHO with a May 21 start date. The variation in r_p displays a distinct pattern, and the magnitude is much smaller as compared to the May 16 orbit. The maximum variation in apse angle is also smaller and retains the 3:1 pattern.

One goal in transitioning to the ephemeris model for various epochs is to consistently produce the "tighter" and more repeatable NRHO trajectory in the ephemeris model regardless of the initial date. As evident in Figure 5, the same stacked orbits in the CR3BP yield different converged solutions in the ephemeris model depending upon the initial date. Given the solution in the CR3BP model, the nodes along the path are dimensionalized and transformed individually into the ephemeris model. Different epoch dates correspond to different dynamical conditions, and the final solution for the same stacking sequence is not the same. One option to address these difference is to alter the stacking pattern given any starting epoch.

Consider the 12 stacked NRHOs from the CR3BP that produce the ordered NRHO in Figure 5. The first node along the path is associated with the start date of May 21, and the remaining nodes along the same trajectory are advanced in time to the corresponding downrange integration time from the first node. The twelve revolutions of the NRHO include 121 nodes (10 nodes per NRHO) in total. A plot of the Julian dates corresponding to the Earth-Moon distance on the date of each node appears in Figure 7a. Given the same stacked set of nodes in the CR3BP, consider transitioning based on a start date of May 16. The first node is now associated with May 16 and the remaining nodes are advanced to dates based on their respective downrange integration times from the first node. The Julian dates for all the nodes and the corresponding Earth-Moon distance are also plotted in Figure 7b. The mismatch between the nodes on the

two dates is apparent from the plots in Figure 7, as the nodes in the trajectories correspond to different Julian dates.

Modifying the starting dates of the nodes for the trajectory starting on May 16 to match more closely with the dates of the nodes for the trajectory starting on May 21 results in a converged trajectory that appears similar to the solution originating on May 21. This adjustment is possible by altering the stacking sequence in the CR3BP before transforming it into the ephemeris model. Rather than stacking one full revolution of the NRHO originating from the *x*-*z* plane as the first orbit, a partial arc of the NRHO is included. The remaining orbits are stacked at the end of the first orbit starting from the *x*-*z* plane. This modification alters the epoch of each node, exactly matching the nodes of the trajectory starting on May 21. The epoch dates of the new sequence match those in Figure 7b.

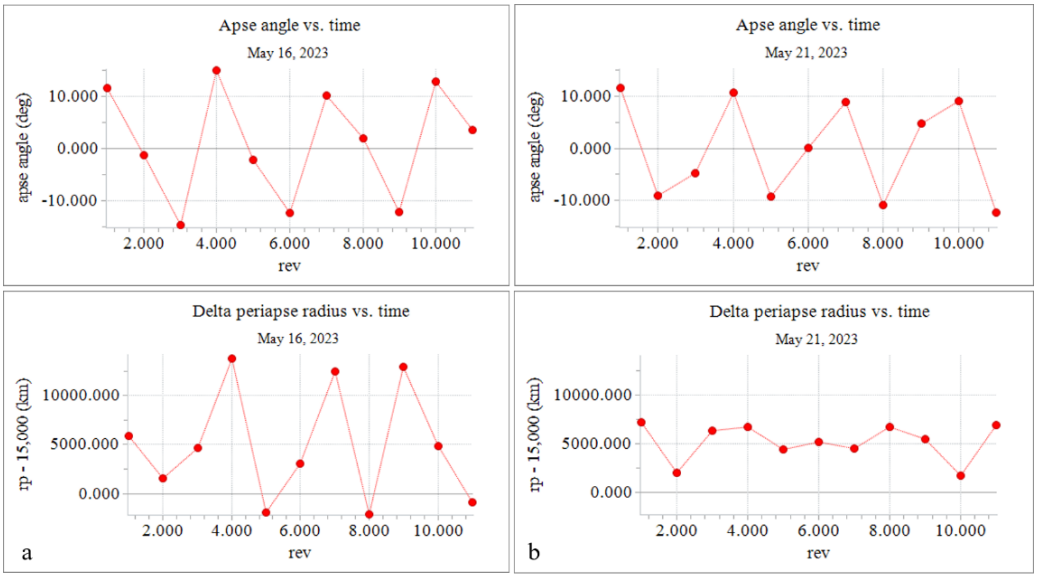

Figure 6. Apse angle vs. time and Δr_p vs. time for two sample 3:1 lunar synodic resonant NRHOs. May 16, 2023 (a) and May 21, 2023 (b).

Applying the same corrections algorithm to this new sequence of nodes in the ephemeris model originating on May 16 results in a converged trajectory that resembles the trajectory originating on May 21, although the first node along the trajectory is no longer aligned with the *x*-*z* plane; the phase has been adjusted. The old and the new corrected trajectories commencing on May 16th appear in Figure 8. The blue markers indicate the first node along the trajectory. From the figure, the transformation from a looser orbit that is more spread out on the left to a tighter path on the right is apparent.

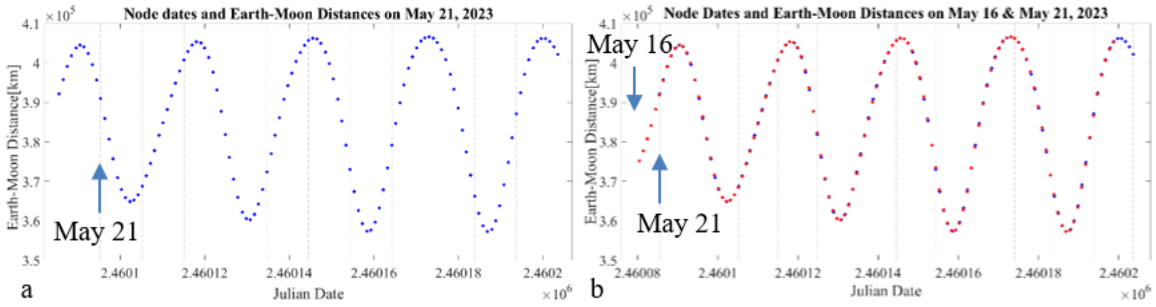

Figure 7. Node dates and Earth-Moon distances for May 21 (a) and May 16 (b)

The phasing can be adjusted for any member of the halo family and over any number of revolutions. For resonant orbits, modification of the phase preserves the geometry to avoid eclipses. In Figure 8, the trajectories are plotted in the Earth-Moon rotating frame (a, c) on the left and in the Sun-Moon rotating

frame (b, d) on the right. The eclipse avoidance strategy typically exploits the 'gaps' along the path in the Sun-Moon rotating frame that are apparent in phased solutions. The phasing procedure is thus helpful to consistently converge to the nearby tighter, less spread out trajectory in the ephemeris model on any given day. This technique is also useful to converge trajectories on days which usually do not converge with the traditional stacking method.

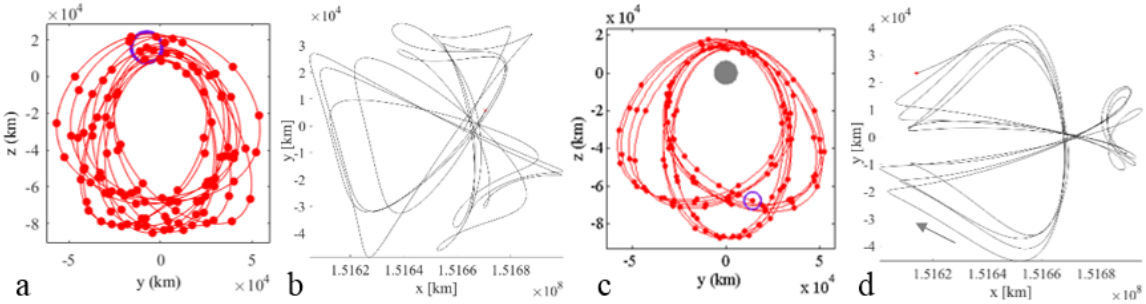

Figure 8. Trajectories commencing on May 16, 2023 with original stacking sequence in the Earth-Moon rotating frame (a) and the Sun-Moon rotating frame (b). Updated sequence in (c) and (d). Initial patch points marked in blue.

Butterfly Orbits

Like the halo orbits, the butterfly orbits are periodic in the CR3BP and exist as quasi-periodic orbits in a higher-fidelity force model. In the current investigation, butterfly orbits are transitioned to the ephemeris model using a two-level targeter in the FreeFlyer software package.[25] With six patchpoints selected per revolution, up to 25 revolutions are stacked to achieve about a year in each butterfly. These butterfly orbits then provide virtual reference orbits for stationkeeping analysis. As with the halo orbits, the epochs of the selected patch points can have a significant effect on the resulting quasi-periodic butterfly. Two samples appear in Figure 9. Three projections of an L_2 southern butterfly orbit with r_p = 2,200 km appear in the top panel, and the same three projections of a larger butterfly with r_p = 8,800 km in the bottom panel. The larger butterfly is in a near 2:1 resonance with the Moon, and the pattern is apparent in the resulting orbit.

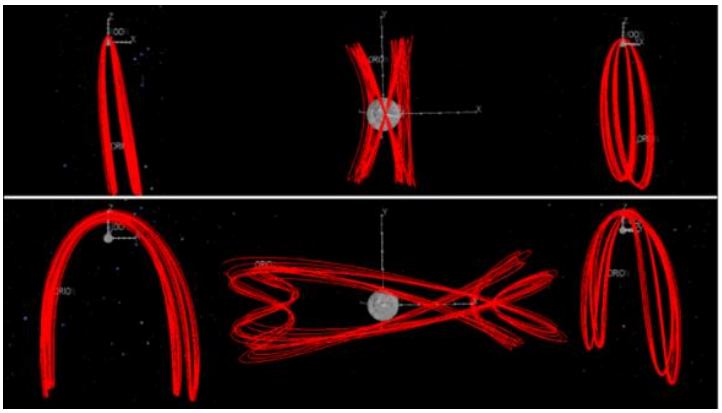

Figure 9. Two L_2 southern butterfly orbits corrected in a high-fidelity model in three projections. Perilune radius r_p = 2,200 km (top) and r_p = 8,800 km (bottom).

HALO ORBIT MAINTENANCE

For a spacecraft exploiting the sensitive dynamics that characterize the halo families, orbit maintenance is required for long-term operations. The halo orbits farther from the Moon are unstable, and even in the NRHOs, which exhibit more stable behavior, perturbations and mismodeling lead to escape over time for an uncontrolled spacecraft. Thus, an orbit maintenance regimen is necessary. Stationkeeping of the Earth-Moon halo families has been explored by several researchers. Analysis in the CR3BP was performed across the L_1 and L_2 families in preparation for the first spacecraft to fly in Earth-Moon halo orbits, the ARTEMIS mission. Both pre-launch[9] and post-mission[12] analysis of the unstable L_1 and L_2 ARTEMIS halos are

documented in higher-fidelity ephemeris force models. Stationkeeping of the L_2 southern NRHOs is considered for DSG applications by Guzzetti et al.[8] and Davis et al.[13] In the current investigation, the L_1 and L_2 halo orbits are explored from a stationkeeping perspective across both families in a high-fidelity force model.

For all analyses considered in the current investigation, the problem of orbit maintenance is divided into two pieces. The first piece consists of generating a long-horizon virtual reference orbit, resulting in a path that retains the general characteristics of the CR3BP halo orbit. The second piece, short horizon stationkeeping, is introduced to correct deviations from the halo orbit behavior due to errors and perturbations. Assume that the spacecraft has been inserted into a virtual reference orbit. As the spacecraft moves along its orbit, it is affected by the initial insertion error and by continuing spacecraft and navigation errors. As the orbit diverges from the desired path, it reaches a specified point in the orbit where a stationkeeping maneuver is executed to direct the spacecraft back towards the desired halo. At this point, a differential corrector is employed to compute the Δv required to achieve specified targets downstream in the orbit. The targeted parameters may be associated with a virtual reference orbit or they may be independent of a reference. An effective strategy for halo stationkeeping depends on several variables, including the location and timing (or phasing) of the targeting maneuvers, the specific constraint targets, and the distance downstream to target the selected constraints.

The plots of orbital periods and stability indices of the L_1 and L_2 halo families in Figure 2 demonstrate that the dynamical properties of the orbits evolve along with the perilune radius values. In addition, as the orbits are transitioned from the CR3BP to the ephemeris model, the variation in apse angle and r_p of the converged quasi-periodic orbits vary, as in Figures 3 and 4. As orbital period, stability, and apse angle properties change across the L_1 and L_2 halo families, stationkeeping algorithms are updated correspondingly for effective and inexpensive orbit maintenance. Three general regions are identified based on varying characteristics of the halo orbits. On both the L_1 and L_2 sides, well-ordered, unstable halo orbits with small variation in apse angles exist from the planar Lyapunov bifurcation to a perilune radius of about 25,000 km. A transition region composed of unstable halos and larger-r_p NRHOs is characterized by large variations in apse angles and exists between 10,000 km < r_p < 22,000 km. The smaller-r_p NRHOs again demonstrate small variations in apse angle and possess perilune radii below 10,000 km. Certain stationkeeping strategies suited for one region may not be effective in other regions. Even within the small-r_p NRHO region, the L_1 and L_2 families demonstrate different behavior and require adjustments to orbit maintenance algorithms.

Navigation and Spacecraft Error Modeling

Orbit maintenance is considered for both crewed and uninhabited spacecraft. In each case, navigation errors and operational noise are simulated. Several combinations of possible errors are applied to estimate lower and upper bounds on expected orbit maintenance costs. Five levels of navigation errors on the state are investigated, with 3σ errors ranging from small values of 0.3 km in position and 0.3 cm/s in velocity to large values of 100 km in position and 100 cm/s in velocity.

Perturbations associated with the spacecraft itself are also included. Two spacecraft configurations are investigated: a quiet spacecraft configuration (no humans present, no attitude deadbanding required) and a noisy spacecraft configuration (humans on board, 3-axis stabilized). The quiet spacecraft configuration includes a fixed maneuver execution error of 0.03 cm/s applied in a random direction and a 5% error on SRP area and 10% error on coefficient of reflectivity (both zero mean, 1σ). For a noisy spacecraft inhabited by humans and 3-axis stabilized, additional errors are assumed. These errors include mismodeling of attitude deadband and slew maneuvers, as well as CO_2 expulsion (Pressure Swing Adapter [PSA] puffs) and wastewater dumps. The magnitude and frequency of noisy spacecraft errors are summarized in Table 1.

Table 1: Noisy spacecraft configuration

Noisy spacecraft errors. Fixed magnitude, random direction.		
Error type	*Magnitude (m/s)*	*Frequency*
PSA puffs	8.3480E-04	every 10 min
Attitude deadbands	2.0043E-05	every 70 min
Attitude slews	6.9751E-04	every 3.2 hours
Wastewater dumps	1.8840E-03	every 3.0 hours

Small-r_p NRHOs

Previous investigations by Guzzetti et al.[8] and Davis et al.[13] explore the problem of stationkeeping L_2 southern NRHOs with perilune radii 2,100 km < r_p < 7,000 km. These investigations consider the orbit maintenance problem from a DSG perspective, considering both quiet, uncrewed spacecraft configurations and noisy, inhabited spacecraft configurations. Two algorithms are explored. A Cauchy-Green Tensor approach exploits dynamical systems theory to select maneuver magnitude and direction, and an *x*-axis crossing control algorithm targets the rotating *x*-velocity of a virtual reference trajectory along a receding horizon. Each of these two algorithms applies a small stationkeeping maneuver approximately once a week near apolune. Both approaches yield low-cost, effective stationkeeping for a spacecraft in a long-term stay in an L_2 southern NRHO.

The current study extends the NRHO analysis to consider L_1 southern NRHOs. The focus is on the *x*-axis crossing control algorithm previously investigated. This stationkeeping method applies a small maneuver near each apolune to target the rotating *x*-velocity v_x along a virtual reference for a set number of revolutions downstream. An approximate maneuver location appears as a blue dot on the 2,300 km NRHO in Figure 3. Applying a single maneuver during each revolution is proven a very effective strategy for the L_2 family. For L_2 southern NRHOs with perilune radii 2,100 < r_p < 9,000 km, a receding horizon of 6.5 revolutions offers reliable and inexpensive orbit maintenance with a single maneuver per revolution for both noisy and quiet spacecraft configurations for a range of navigation error levels.

By contrast, the L_1 southern NRHOs, while similar in appearance, exhibit different behavior. Three differences in orbit characteristics are immediately apparent: the L_1 family exists in closer proximity to the Earth, the L_1 NRHOs possess larger apolune radii as r_p decreases (see Figure 1), and their stability indices are larger (see Figure 2b). These differences are particularly important for small-r_p L_1 NRHOs. For L_1 NRHOs with perilune radii 2,000 < r_p < 7,000 km, a single maneuver that targets v_x is ineffective for long-term stationkeeping. By contrast, a single maneuver that targets both v_x and perilune radius r_p is highly effective; however, with a simple targeter seeking a feasible solution, targeting both parameters with a single maneuver yields unnecessarily high costs. Instead, two maneuvers per revolution are implemented. Both maneuvers target the rotating *x* velocity v_x of the virtual reference NRHO at perilune. The maneuvers are placed on either side of apolune, at osculating true anomaly values before apolune of 140° or 150° and after apolune of 200° or 210°, as represented by the blue dots on the 4,000 km NRHO in Figure 4. At the smallest r_p values considered, 2,000 km < r_p < 6,000 km, the receding horizon for targeting is selected to be one half revolution ahead. That is, the maneuvers before and after apolune target v_x at the subsequent perilune passage; longer targeting horizons result in a less reliable algorithm (more failed cases) for these orbits. For NRHOs with 7,000 < r_p < 9,000 km, a longer horizon is found to be robust, and a targeting horizon of 4.5 revolutions is selected to reduce total stationkeeping cost. That is, the maneuvers before and after apolune target v_x at perilune along the reference trajectory 4.5 revolutions downstream. For this 7,000 to 9,000 km subset of the L_1 NRHOs, the single-maneuver algorithm applied to the L_2 NRHOs also results in reliable stationkeeping.

The mean annual stationkeeping costs for the L_1 and L_2 southern NRHOs with perilune radii 2,000 km < r_p < 9,000 km appear in Figure 10 for three navigation error levels. Each data point represents a 500-trial Monte Carlo run, with each trial propagated for 30 revolutions. The L_2 NRHOs, in Figure 10b, all have a relatively long targeting horizon of 6.5 revolutions. The trend in annual Δv as a function of perilune radius is smooth for all three error levels, and for each, the curve has a maximum around 8,000 km. As expected, larger navigation errors lead to larger costs. The L_1 NRHOs appear in Figure 10a. Of the three error levels considered, the smaller two lead to similar patterns in stationkeeping cost. The trend is less smooth than in the L_2 family, due in part to the changing targeting horizon. For the highest r_p values considered here, the targeting horizon is 4.5 revolutions, and the mean cost is only slightly higher than the corresponding L_2 NRHO. For L_1 NRHOs with r_p values 6000 km and below, however, the cost increases due in part to the short, half-revolution targeting horizon required to ensure reliable orbit maintenance. For the largest error level considered in this section, 10 km in position and 10 cm/s in velocity (3σ), the pattern is significantly different for the L_1 NRHOs. The mean costs range from 10-16 m/s annually with a minimum at r_p = 6,000 km. For each data point represented in Figure 10, the 500-trial Monte Carlo runs result in 100% success. Note that for the largest navigation error level considered for the small-r_p NRHOs, 10 km in position and 10 cm/s in velocity (3σ), data does not appear for L_1 halos with r_p = 2,000 km and r_p = 9,000 km. The larger

navigation errors result in impacts in many trials for L_1 halos with r_p = 2,000 km with the x-axis crossing control algorithm, and result in escapes in many trials for L_1 NRHOs with r_p = 9,000 km.

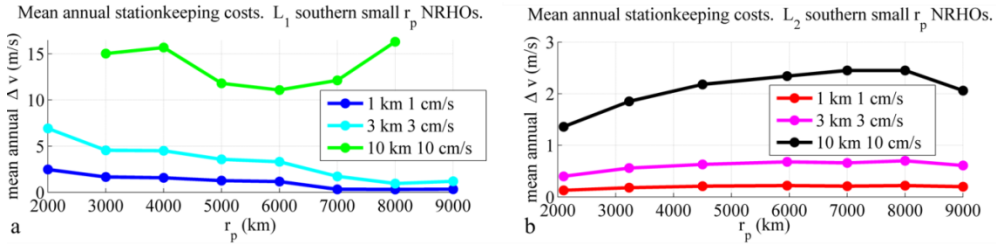

Figure 10. Mean annual stationkeeping costs for L_1 (a) and L_2 (b) small-r_p southern NRHOs for 3 navigation error levels; quiet spacecraft configuration

The stationkeeping costs for the L_1 and L_2 NRHOs are roughly aligned with the stability indices computed in the CR3BP analysis. In Figure 11, stability indices for the L_1 and L_2 NRHOs appear in blue and red respectively in the top plot, and the mean annual stationkeeping costs appear in the bottom plot for low navigation errors and a quiet spacecraft configuration. In both plots, the L_1 values are higher than L_2, and decrease as r_p grows. The L_2 values, on the other hand, slowly increase to a maximum around 8,000 km and then begin to decrease. Not surprisingly, orbit maintenance costs tend to be higher for trajectories associated with higher stability indices.

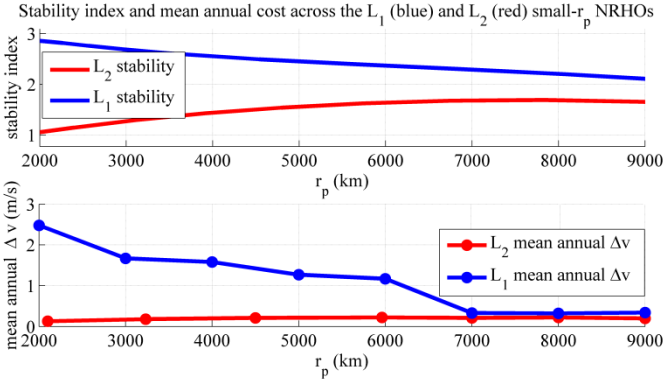

Figure 11. Stability index (top) and mean annual stationkeeping cost (bottom) for the L_1 and L_2 small-r_p southern NRHOs. Quiet spacecraft configuration, low navigation errors.

Transition Region

As perilune radius values increase beyond 9,000 km, stability indices in both the L_1 and L_2 halo families fall, as in Figure 2b, suggesting that stationkeeping costs should also fall. However, other factors arise and affect the cost and reliability of orbit maintenance. As demonstrated in Figure 3, as the perilune radii of the halo orbits increase, the range of apse angles tends to increase as well when the orbits are transitioned into a higher-fidelity force model. A transition portion of the halo family is comprised of orbits characterized by large apse angles. Halos in both the L_1 and L_2 families with perilune radii 10,000 km < r_p < 22,000 km fall into the transition group. Variations in orbital characteristics from one revolution to another along the virtual reference lead to challenges as errors are added to the spacecraft trajectory. As the trajectory diverges from the virtual reference due to navigation and spacecraft errors over time, the reference is a decreasingly accurate model of the spacecraft orbit. In addition, the period of the halos increases along with perilune radius. Thus, despite the low stability indices of these halos, *x*-axis crossing control with a single maneuver per revolution ceases to effectively control a spacecraft in this region over long-term propagation, even in the L_2 family, which is effectively controlled with a single maneuver per revolution for smaller-r_p NRHOs.

Identifying a single stationkeeping algorithm based on *x*-axis crossing control that effectively maintains a spacecraft in any halo orbit in the transition region is not straightforward. Instead, care must be taken to select a baseline trajectory that is conducive to long-term orbit maintenance. As described previously, by

changing phasing of patch points, a reference trajectory can be selected with particular characteristics. However, it is worth noting that a reference orbit characterized by relatively small variations in apse angle and perilune radius will not necessarily respond well to a given orbit maintenance algorithm, even if that algorithm effectively controls a reference that is similar in appearance. In addition, the particular revolution selected for orbit insertion affects both cost and reliability of the stationkeeping algorithm, sometimes significantly.

However, careful selection of the virtual reference can lead to reliable and inexpensive stationkeeping. For example, two sample L_2 halo references with r_p = 15,000 km and starting epochs on May 13 and May 20, 2023 lead to 100% success and mean annual stationkeeping costs below 1 m/s with a quiet spacecraft configuration and navigation errors of 0.3 km and 0.3 cm/s (3σ). Nearby references, on the other hand, yield much higher costs and significantly lower success rates. Five samples appear in Figure 12. Similar patterns are seen in the transition region of the L_1 family.

While *x*-axis crossing control can effectively and inexpensively maintain a spacecraft in a carefully selected virtual reference within the transition region of the halo families, a different stationkeeping strategy may be more effective for a wider range of virtual reference options.

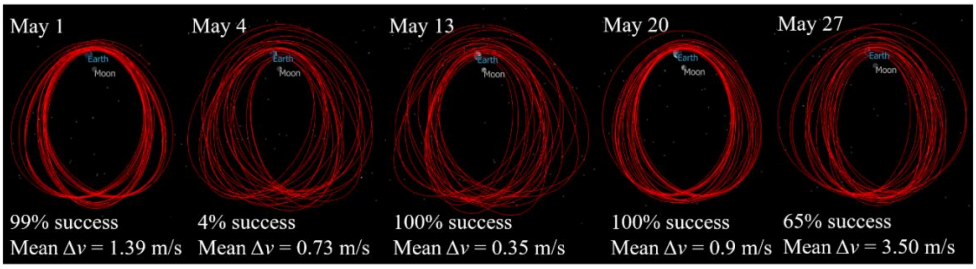

Figure 12. Five L_2 NRHOs with r_p = 15,000 km in May 2023.

Unstable Halo Orbits

In both the L_1 and L_2 families, the portions of the halo family with r_p > 25,000 km are characterized by large stability indices and can achieve small variations in apse angle when converted to a high-fidelity force model. The orbits flown by the ARTEMIS spacecraft exist in this unstable region. Despite the high stability indices, robust and inexpensive stationkeeping is achievable with careful algorithm selection. In this study, the focus is on a continuation method that employs *x*-axis crossing control; several variations are considered. As in the analysis described above, the *x*-axis crossing control algorithm implemented for the unstable halos employs a virtual baseline trajectory that represents the desired spacecraft behavior. In the implementation explored here, two maneuvers are employed to control the unstable halo orbits. Since the orbital periods of the unstable halos range from about 12 to 15 days (see Figure 2), the burns occur approximately once a week, as in the L_2 small-r_p NRHO algorithm described above. The maneuvers are placed at the northern, positive *x*-axis crossing and the southern, negative *x*-axis crossing, as illustrated by blue dots on the 40,000 km L_2 halo in Figure 3 and the 44,000 km L_1 halo in Figure 4.

Four variations on *x*-axis crossing control are explored with a quiet-spacecraft configuration. The first algorithm targets the rotating *x*-velocity of the virtual reference orbit a half revolution ahead at the subsequent *x*-axis crossing. The Δ*v* direction and magnitude are free to vary to design a feasible maneuver that achieves a spacecraft rotating *x*-velocity equal to that along the virtual reference trajectory at the target point half a revolution ahead. The other five components of the spacecraft state are unconstrained. The spacecraft is then propagated ahead to the next *x*-axis crossing, and the process is repeated. A feasible stationkeeping solution is thus achieved. However, by directing the velocity in a particular direction, improvements to the feasible solution are available. It was discovered during ARTEMIS operations that the optimized stationkeeping maneuvers were well aligned with the stable-mode direction of the halo orbit itself. That is, the eigenvector direction associated with the real eigenvalue of the monodromy matrix $\lambda < 1$ matched well with each optimized maneuver.[12] In the current investigation, a second strategy thus constrains the Δ*v* direction to be aligned with the stable mode of the monodromy matrix associated with the corresponding CR3BP halo orbit while targeting a half revolution ahead.

When designing a maneuver to target certain trajectory behavior, a longer targeting horizon can reduce maneuver cost. In these cases, targeting farther ahead is desirable. However, because the halo orbits

characterized by large r_p values exhibit unstable behavior, a spacecraft will quickly escape from the vicinity of the halo orbit during propagation in a long-horizon targeting process. To reliably target more than half a revolution ahead without escape in the presence of spacecraft and navigation errors, a continuation method is employed. Similar to the method developed by Folta et al.,[7] the continuation method first targets a half revolution ahead to the reference *x*-velocity. The resulting maneuver is used as an initial guess for a maneuver targeted a full revolution ahead. The next result then seeds the targeter to compute a Δv to achieve a rotating *x*-velocity equal to the reference value 1.5 revolutions ahead. The process can be continued for several revolutions, and it can employ a free maneuver direction or it can constrain the maneuver to the stable mode direction. These two variations represent a third and fourth orbit maintenance method explored for quiet spacecraft.

Mean annual orbit maintenance costs across the unstable portion of the L_2 halo family for the four variations on the *x*-axis crossing control algorithm appear in Figure 13. Each data point represents a 500-trial Monte Carlo run. In each run, the spacecraft orbit is maintained for 17.5 revolutions, equivalent to 208 to 259 days. A quiet spacecraft configuration is considered with low navigation errors of 1 km in position and 1 cm/s in velocity (3σ). At the maximum perilune radius of about 51,000 km, the halo orbits are nearly in plane, and the four variations yield approximately the same annual cost, about 3.2 m/s. As the family evolves out of plane, the benefits of targeting farther ahead become apparent. Targeting a half revolution ahead yields the blue curve with a free maneuver direction and the red curve when the maneuvers are constrained to the stable mode direction. These two curves increase to a maximum of 3.5 m/s before decreasing to around 2 m/s annually at about 30,000 km r_p. As the halo family approaches the transition region characterized by larger apse angles, costs increase significantly when targeting half a revolution ahead. The method ceases to effectively maintain a spacecraft in a long-term orbit for halos with $r_p <$ 25,000 km. Except for the nearly planar halo at r_p = 51,000 km, targeting farther ahead is consistently less expensive. The green and black curves represent variations on the *x*-axis crossing algorithm that use continuation to target 1.5 or 2.5 revolutions ahead. The annual costs for these methods decrease along with the stability index to a minimum of about 1.3 m/s at r_p = 25,000 km. For $r_p <$ 22,000 km, the methods begin to fail as the halos approach the transition region characterized by large apse angles.

Constraining the maneuver direction to lie along the stable mode direction decreases the annual stationkeeping cost in almost every case, a result supporting the ARTEMIS observation that the optimal maneuvers are aligned with the stable mode. The difference in cost is small between the constrained and free maneuver directions. Note that for the nearly-stable NRHOs, the stable mode direction is not well defined, and a decrease in cost is not observed when constraining the maneuver to the stable direction.

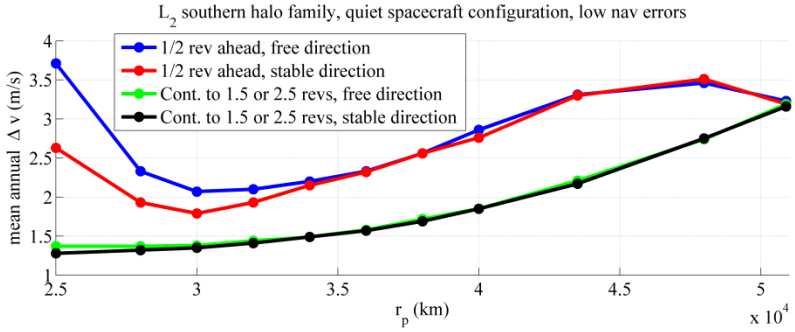

Figure 13. Annual stationkeeping cost across the unstable L_2 southern halos. Quiet spacecraft configuration, low navigation errors. Four stationkeeping algorithm variations.

Costs for the four variations on *x*-axis crossing control are considered for a range of navigation errors. Results for the five navigation error levels for noisy and quiet spacecraft configurations for a single method appear in Figure 14. The selected method employs continuation to 1.5 or 2.5 revolutions and constrains maneuver direction to the stable mode. Not surprisingly, higher navigation errors lead to higher stationkeeping costs. At low navigation error levels, the spacecraft noise dominates the cost. As the navigation errors increase, however, the differences between noisy and quiet spacecraft errors diminish. At navigation errors levels of 10 km in position and 10 cm/s in velocity (3σ), stationkeeping costs are nearly equal for noisy and quiet spacecraft configurations. This result is consistent with the L_2 NRHO results in Guzzetti et al.[8] and Davis et al.[13]

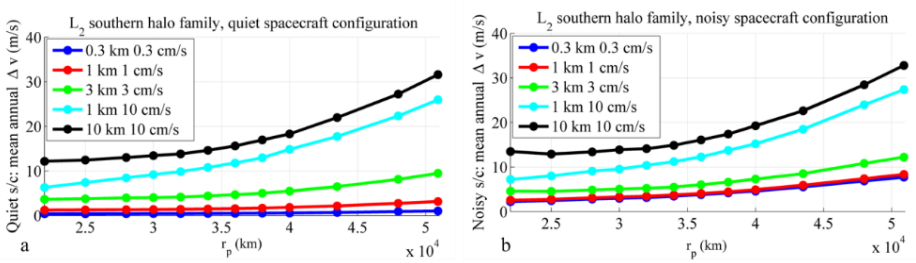

Figure 14. Annual stationkeeping cost across the L_2 southern unstable halos. Continuation to 1.5 or 2.5 revolutions with maneuvers in the stable mode direction. Varying navigation error levels. Quiet spacecraft configuration (top) and noisy spacecraft configuration (bottom).

Thus far, the results shown in this investigation represent the mean stationkeeping errors for each 500-trial Monte Carlo run. However, the minimum and maximum expected annual costs are also of interest. Minimum annual cost (in blue) and maximum annual cost (in green) appear along with the mean cost (in red) for a representative case in Figure 15. The selected case employs continuation to 1.5 or 2.5 revolutions with a quiet spacecraft configuration and low navigation errors. The mean cost shows a very smooth trend as r_p varies. As expected, more variations are seen in the minimum and maximum values.

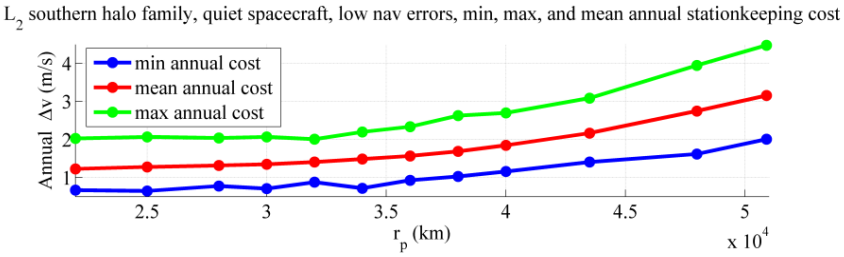

Figure 15. Minimum, maximum, and mean annual stationkeeping costs across the L_2 southern unstable halos. Continuation to 1.5 or 2.5 revolutions with maneuvers in the stable mode direction for a quiet spacecraft configuration and low navigation errors.

During ARTEMIS operations, the orbit maintenance scheme targeted a small value of v_x rather than a reference value,[9] removing the need for a virtual baseline trajectory. For noisy spacecraft, a comparison is made between targeting a small arbitrary value of v_x via continuation 1.5 revolutions ahead vs. targeting the reference v_x with the same algorithm. Across the unstable L_2 southern halo orbits, the mean annual costs for navigation errors of 1 km in position and 1 cm/s in velocity (3σ) appear in Figure 16. For halos with r_p > 36,000 km, the two methods yield approximately equal mean stationkeeping costs. For lower values of r_p, however, targeting to a virtual reference yields significantly improved results.

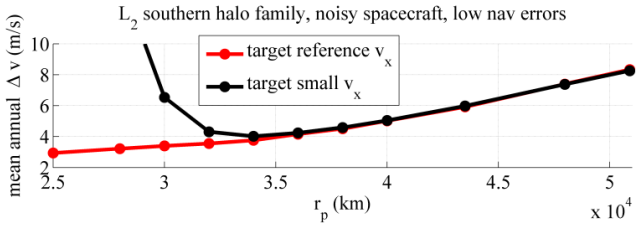

Figure 16. Mean annual stationkeeping costs across the L_2 southern unstable halos. Continuation to 1.5 revolutions with free maneuver direction. Targeting the reference v_x (red) and a small arbitrary value of v_x (black).

Similar trends appear across the L_1 unstable halo orbits. Again, sets of 500 Monte Carlo trials are run for halo orbits in the L_1 southern family with 25,000 km < r_p < 51,000 km. Each halo orbit is maintained for 17.5 revolutions. Six levels of navigations errors are explored for both noisy and quiet spacecraft. A continuation scheme is employed to target 2.5 revolutions downstream for quiet spacecraft and 1.5 revolutions ahead for noisy spacecraft. Mean annual stationkeeping costs for the L_1 unstable halos appear

for both noisy and quiet spacecraft configurations for five levels of navigation error in Figure 17. With navigation errors of 10 km in position and 10 cm/s in velocity (3σ), there is little difference in cost for a noisy spacecraft configuration as compared to a quiet spacecraft; the navigation errors dominate the orbit maintenance costs. As navigation errors decrease, the effects of noise on the spacecraft become more apparent.

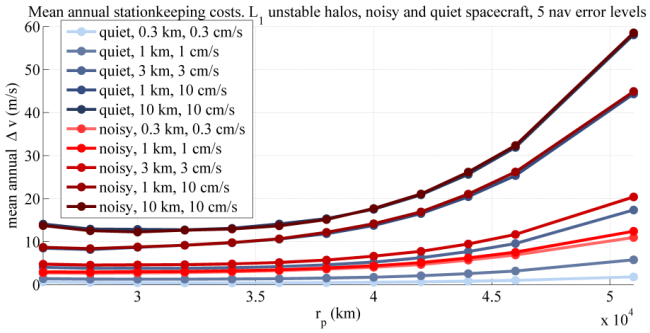

Figure 17. Mean annual stationkeeping costs across the L_1 unstable halos. Noisy spacecraft configuration in shades of red, quiet configuration in blue, 5 navigation error levels (3σ).

A comparison between mean annual stationkeeping costs for quiet spacecraft with low navigation errors appears in the bottom plot in Figure 18 for the two halo families. For large values of r_p, costs are higher for the L_1 family. The costs decrease as the halos grow out of plane, with orbit maintenance costs in the L_1 family decreasing faster. The costs for the L_1 and L_2 families meet at an approximate perilune radius of r_p = 42,000 km. In the top panel of Figure 18, the stability indices for the L_1 and L_2 halo families appear as computed in the CR3BP. Clearly, the mean annual costs, appearing in the bottom plot, mirror closely the stability indices of the two halo families, shown in the top plot.

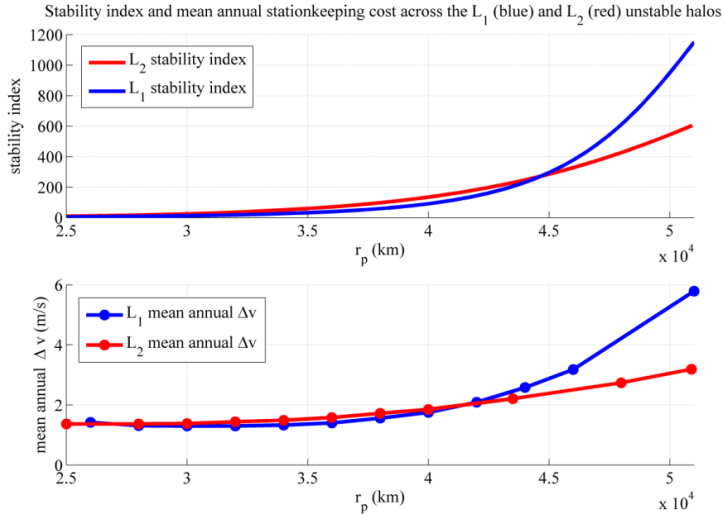

Figure 18. Stability index (top) and Mean annual stationkeeping cost (bottom) for the L_1 and L_2 unstable halos. Quiet spacecraft configuration, low navigation errors.

Butterfly Orbits

Bifurcating from the L_2 NRHOs, the butterfly orbits share some NRHO characteristics, including low values of stability index and small perilune radii. Not surprisingly, orbit maintenance algorithms that are effective for the NRHOs also prove reliable for members of the butterfly family. An *x*-axis crossing control algorithm is again selected for analysis. Since the butterflies possess two lobes that wrap around the Moon, a small orbit maintenance maneuver is placed near apolune at each half-revolution. As in the NRHO algorithm, the maneuver targets the rotating *x*-component of velocity 6.5 *x*-axis crossings downstream at perilune along a virtual reference trajectory. Since a butterfly passes through perilune twice per revolution, the targeting horizon is equivalent to 3.25 full revolutions.

Several sample butterfly orbits are investigated to explore stationkeeping costs. For butterflies with smaller perilune radii, a single maneuver per half revolution is selected, analogous to the once-per-rev stationkeeping strategy effective for the L_2 NRHOs. However, as the perilune radius increases and apolune decreases, a double maneuver strategy, similar to that applied to the L_1 NRHOs, yields lower costs for the butterfly orbits. For each case, 500 Monte Carlo trials are run for 42 half revolutions, or 255-284 days. Mean annual costs for four sample butterfly orbits appear in Figure 19 for a quiet spacecraft configuration and three navigation error levels. The costs increase as perilune radius increases, mirroring the trend in stability index (see Figure 2c).

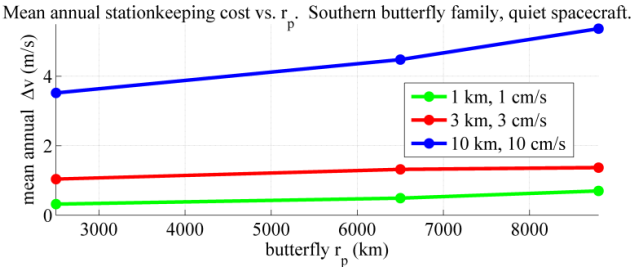

Figure 19. Mean annual stationkeeping cost vs. perilune radius across the L_2 southern butterfly family. Quiet spacecraft configuration, three navigation error levels.

CISLUNAR TRANSFER DESIGN

One of the proposed purposes of the DSG is to serve as a proving ground for human spaceflight operations in deep space. With this goal in mind, the DSG plans to execute long-term excursion missions from the NRHO to other orbits in cislunar space. Destination orbits under consideration include the DRO, other L_1 and L_2 Halo orbits, and Butterfly orbits. Thus, transfers are required between these cislunar orbits. The use of Poincaré maps for locating trajectories that connect two different periodic orbits (heteroclinic connections) or that depart and then return to the same periodic orbit (homoclinic connections) via stable and unstable manifold trajectories is well documented. Notably, Haapala and Howell[26,27] employ multi-dimensional Poincaré maps for generation of homoclinic and heteroclinic connections between halo and vertical orbits in the spatial problem. Frequently, these connections are identified using a Poincaré map that defines a surface of section in configuration space centered on P_2. However, periapsis Poincaré maps can also be used to locate connecting transfers between periodic orbits.[12,28] In the current study, the Deep Space Trajectory Explorer (DSTE) software is extended to generate Poincaré maps representing transfers across a range of maneuver magnitudes and directions. Maps representing transfers departing the originating orbit are overlaid on maps corresponding to transfers approaching the destination orbit to find intersections. The potential transfers are then corrected in the Copernicus optimization software to find continuous transfer orbits.

NRHO to Unstable Halo Transfers

Commonly, transfers between orbits in the multibody regime are achieved by connecting stable and unstable manifold trajectories between the orbits. However, NRHOs are stable, or nearly so, and butterfly orbits also demonstrate nearly stable behavior. Thus, they do not possess useful manifolds for trajectory design. In previous investigations,[26] transfers between NRHOs and other orbits are found in the DSTE through a transfer generator that allows the user to select a single impulsive maneuver magnitude and a single maneuver direction from a predetermined set. The maneuver is applied at points along a trajectory and generates orbits departing from or arriving at the selected trajectory. In the current investigation, the DSTE is updated to massively generate transfer trajectories that depart from or arrive at an arbitrary selected orbit for user-defined ranges of Δv magnitude and direction. The DSTE's Batch Transfer Generator is developed as a multi-layered visualization providing GUI interfaces for specifying parameter ranges for impulsive maneuvers. To define the maneuvers, the user specifies the minimum, maximum, and step size for ranges of Δv magnitude, yaw, and pitch. These ranges span the maneuver design space for a given application. The user then specifies initial states along a base trajectory, and the Δv is applied at each selected state. The range approach creates a huge combinatorial space of transfers to be integrated. To address the large design space computationally, the DSTE leverages the Java 8 Parallel Streams API to take

advantage of available processors while minimizing thread switching overhead. The parallelization necessitates precomputation of all potential initial conditions using the specified ranges of maneuver parameters prior to the execution of the parallel stream integration. For larger design spaces, the DSTE has the capability to request and submit the maneuver design space parameters to the DSTE Cloud Service, which can be arbitrarily scaled both in available processors and heap memory. To mitigate the overwhelming data space the computations produce, the DSTE Cloud Service has options to sort and filter the resulting transfer trajectory space by several key trajectory design variables specified by the user. As the filtration completes, the reduced subset of preferred transfers is asynchronously streamed back to the client for visualization and data collection. The DSTE gives the user the option to view each transfer trajectory or to return a Poincaré map representing each transfer trajectory.

The Batch Transfer Generator facilitates the design of transfers between an NRHO and an unstable halo orbit. One sample transfer appears in Figure 20. The origin orbit is a 9:2 lunar synodic resonant NRHO. The destination is a northern L_2 halo with r_p = 40,000 km. An initial discontinuous transfer between the two orbits is generated from two Poincaré maps in the DSTE. The first map represents a stable manifold that approaches the L_2 unstable halo orbit. The second map is generated using the Batch Transfer Generator, with a range of maneuver magnitudes and directions for departure locations around the NRHO. The two maps appear overlaid in Figure 20a. Both are *x-y* projections of 3D Poincaré maps. Points that align in the projection must also align in the z-direction to be continuous in space; if the velocity direction is also aligned, a low-cost transfer is identified. One potential transfer is identified by a circle in Figure 20a. A click on the NRHO transfer periapsis map propagates a selected point backwards to the NRHO; a click on the halo manifold map propagates forward to the unstable halo orbit. The resulting four segments (NRHO, transfer segment, manifold segment, halo) appear in Figure 20b. A discontinuity appears in the upper left—this discontinuous orbit in the DSTE serves as an initial guess for a continuous transfer. The trajectory segments are exported to Copernicus, where SNOPT is employed to generate a locally optimal, continuous transfer between the NRHO and the unstable halo orbit in a CR3BP force model. This transfer, with a time of flight of 69 days, costs 180 m/s over four maneuvers: one maneuver each to depart the NRHO and arrive at the halo, and two mid-course corrections. The transfer is subsequently further optimized by Ocampo.[29] Several optimized, impulsive-maneuver solutions in the CR3BP force model are then transitioned to a low-thrust, higher-fidelity force model by McGuire et al.[30]

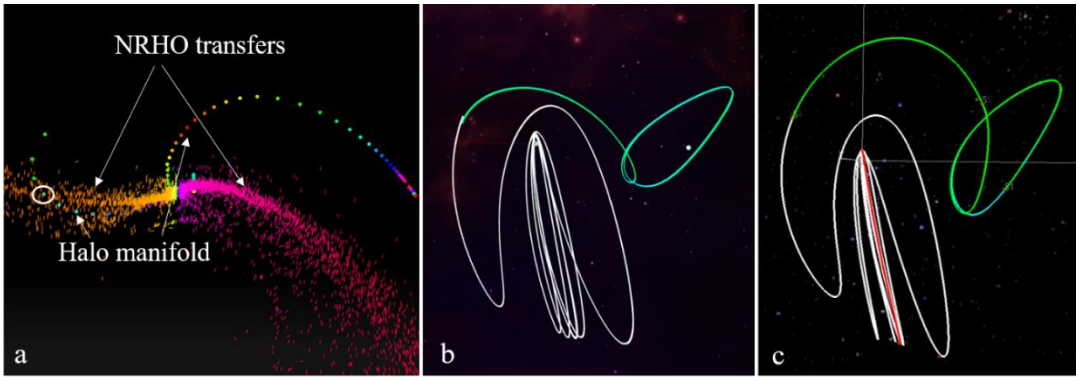

Figure 20. Overlaid periapsis Poincaré maps identify intersecting orbits. (a) Initial guess in DSTE (b). Continuous, locally optimal NRHO to halo transfer in Copernicus (c).

NRHO to Butterfly Transfers

In a similar fashion, the transfer generator in DSTE provides an initial guess for an NRHO to butterfly transfer. Both the primary and destination orbits are nearly stable, so manifold trajectories are not employed for design. Selecting a 9:2 lunar synodic resonant NRHO as the departure orbit and a 3,500 km butterfly as the first destination orbit, an initial guess is found in the DSTE and then converged using Copernicus. A lunar flyby is employed to change the direction of motion at perilune; in the NRHO, the perilune velocity is nearly entirely in the rotating *y* direction, while the velocity of the butterfly at perilune has a significant *x*-component as well. The resulting transfer, optimized using SNOPT in Copernicus, appears in two projections in Figure 21a. Three maneuvers are employed: one to depart the NRHO, one to arrive at the

butterfly orbit, and one mid-course correction. The time of flight is 6.4 days, and the Δv totals 88 m/s. This single-lunar-flyby transfer to a 3,500 km butterfly orbit is then used to seed a continuation scheme that generates a family of similar single-flyby transfers to butterfly orbits with r_p values up to 12,000 km. The times of flight are nearly constant at 6.2 to 6.4 days, and the cost of the transfers, in Figure 22, increases as the butterfly r_p grows, to a maximum of 197 m/s at the largest butterfly orbit. Three sample transfers appear in two projections in Figure 21. The transfers retain a similar geometry as the butterfly r_p grows.

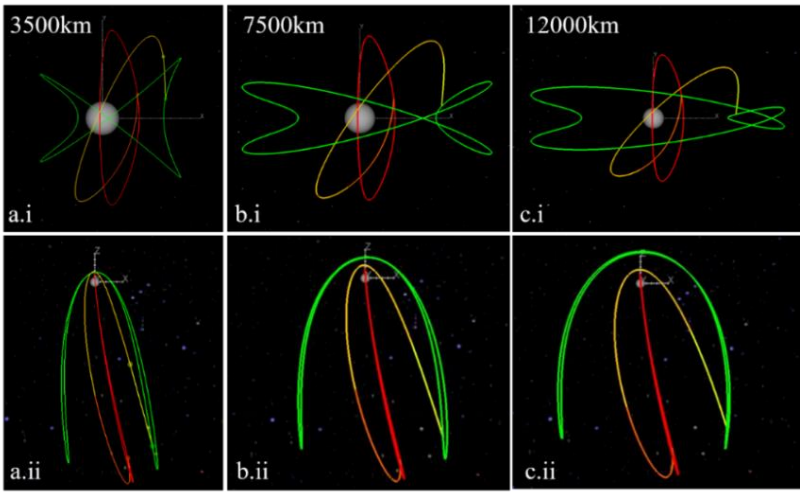

Figure 21. Converged single-flyby transfers from 9:2 lunar synodic resonant L_2 southern NRHO (red) to L_2 southern butterflies (green). To 3,500 km (a), 7,500 km (b), and 12,000 km (c) butterflies.

As always, interest exists in exploring lower-cost options for NRHO to butterfly transfers. To decrease the cost, a longer transfer with two lunar flybys is considered. The design process again begins with a transfer from the 9:2 lunar synodic resonant NRHO to a butterfly orbit with r_p = 3,500 km. Only two maneuvers are employed—one to depart the NRHO and one to arrive at the butterfly. The cost is cut approximately in half in comparison with the single-flyby transfer, with a total Δv of 43 m/s connecting the two orbits. The time of flight is nearly tripled to 17.3 days. The two-flyby transfer to a 3,500 km butterfly appears in two projections in Figure 23a. Again, a continuation scheme is employed to step up the perilune radius of the destination butterfly. Three resulting transfers appear in Figure 23, with similar geometry appearing in the transfers across the family. The times of flight range from 16.5 days to 17.3 days, with the shorter times of flight corresponding to the butterfly orbits with higher perilune radii. The cost increases as the butterfly r_p increases, from 43 m/s for r_p = 3,500 km to 102 m/s for r_p = 12,000 km.

The transfer costs across the two families follow smooth curves, in both cases increasing as the perilune radii of the destination butterfly orbits increase. The Δv for each family appears as a function of butterfly r_p in Figure 22. In contrast, the times of flight for each family remain fairly constant, about 6 days for the single-flyby family and between 16.5 and 17.3 days for the double-flyby family. The existence of smooth families of transfer solutions with predictable behavior between a primary NRHO and destination butterflies suggests that changes to mission requirements may be achieved without significant changes to the baseline trajectory.

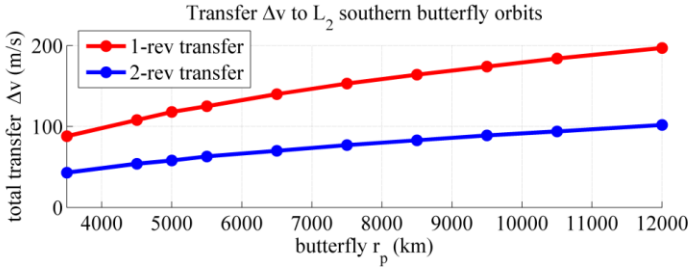

Figure 22. Total transfer Δv for single-revolution (red) and double-revolution (blue) transfers from a 9:2 lunar synodic resonant NRHO to butterfly orbits across the family.

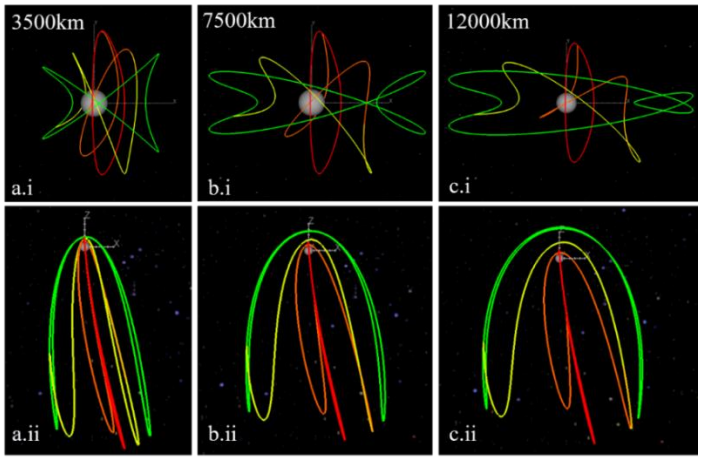

Figure 23. Converged double-flyby transfers from 9:2 lunar synodic resonant L_2 southern NRHO (red) to L_2 southern butterflies (green). To 3,500 km (a), 7,500 km (b), and 12,000 km (c) butterflies.

SUMMARY AND CONCLUDING REMARKS

The Deep Space Gateway is planned to inhabit a long-term orbit in cislunar space, taking advantage of multibody dynamics to facilitate transfers throughout the Earth-Moon system and beyond. The current baseline DSG orbit is an NRHO in a 9:2 lunar synodic resonance around the Moon, but other libration point orbits are considered as potential destination orbits for the DSG and Orion. Other NRHOs in the L_1 and L_2 families and unstable halo orbits in both families are candidate destinations. Resonant NRHOs, such as 3:1 and 4:1 lunar synodic resonant NRHOs, have particularly favorable eclipse avoidance properties, and the unstable halos offer attractive options for transfers to and from Earth and other orbits, including abort opportunities. Butterfly orbits are under investigation for lunar surface access. To explore the accessibility of these various orbits, this investigation focuses on the halo and butterfly families.

When transitioning a periodic orbit in the CR3BP to the ephemeris model, the resulting quasi-periodic orbit can be adjusted with careful selection of patch points and tuning parameters, leading to desirable characteristics for eclipse avoidance. The resulting higher-fidelity reference serves as a virtual baseline for stationkeeping applications. Across the halo and butterfly families, the cost of maintaining a spacecraft in long-term orbit generally scales with the stability index. Higher navigation and noise values logically lead to higher stationkeeping costs. Effective strategies vary across the families, changing along with characteristics of the orbits. For unstable halo orbits far from the Moon, an *x*-axis crossing control algorithm that performs two maneuvers per revolution and employs a continuation process to target ahead 1.5 or 2.5 revolutions to v_x along a virtual reference offers reliable and low-cost orbit maintenance. The cost is improved when the maneuver direction is constrained to align with the stable mode direction associated with the CR3BP periodic orbit. The low-r_p NRHOs demonstrate nearly stable behavior. The L_2 NRHO family is effectively controlled with a single maneuver per revolution at apolune, targeting to perilune 6.5 revolutions downstream. The L_1 family performs better with two maneuvers per revolution, one on either side of apolune, and a shorter targeting horizon. The stationkeeping costs and reliability of a transition region, characterized by perilune radii 10,000 km < r_p < 22,000 km, that exists between the unstable halos and the low-r_p NRHOs, are driven by the careful selection of a reference trajectory. For well-behaved references, inexpensive and robust stationkeeping is achieved by an *x*-axis crossing control algorithm that performs two maneuvers per revolution.

To transfer the DSG into potential destination orbits, periapsis Poincaré maps are employed to generate initial guesses for continuous transfer trajectories. Sample NRHO to unstable halo transfers are designed, and two families of NRHO to butterfly orbit transfers are generated, with smooth trends in Δv and nearly constant values of time of flight. These CR3BP, impulsive transfers will act as initial guesses for high-fidelity low-thrust analysis.

Future analysis will further explore the halo transition region, investigating the characteristics of the variations in apse angle and r_p and how they relate to orbit stability and stationkeeping costs. Alternative algorithms may be better suited to consistently maintaining these orbits over long-term stays.

ACKNOWLEDGMENTS

The authors would like to thank Ryan Whitley, Jacob Williams, and Cesar Ocampo for their insight and assistance. Portions of this work were completed at NASA JSC and Purdue University through contract #NNJ13HA01C and grant #NNX13AK60A, respectively.

REFERENCES

[1] Hambleton, Kathryn. "Deep Space Gateway to Open Opportunities for Distant Destinations." NASA, 28 March 2017. Web.
[2] Whitley, R. and R. Martinez, "Options for Staging Orbits in Cislunar Space," IEEE Aerospace 2015, March 2015.
[3] Szebehely, Z., *Theory of Orbits: The Restricted Problem of Three Bodies*, Academic Press, New York, 1967.
[4] Marchand, B., K. Howell, K., and R. Wilson, "An Improved Corrections Process for Constrained Trajectory Design in the n-Body Problem," Journal of Spacecraft and Rockets, Vol. 44, No. 4, July-August 2007, pp. 884-897.
[5] Wawrzyniak, G., and K. Howell, "Numerical Techniques for Generating and Refining Solar Sail Trajectories," Advances in Space Research (ASR) Special Issue: "Solar Sailing: Concepts, Technology, Missions," Vol. 48, Issue 11, 2011, pp. 1848-185.
[6] Williams, J., D. E. Lee, R. L. Whitley, K. A. Bokelmann, D. C. Davis, and C. F. Berry, "Targeting Cislunar Near Rectilinear Halo Orbits for Human Space Exploration," 27th AAS/AIAA Space Flight Mechanics Meeting, February 2017.
[7] Folta, D., T. Pavlak, K. Howell, M. Woodard, and D. Woodfork, "Stationkeeping of Lissajous Trajectories in the Earth-Moon System with Applications to ARTEMIS," AAS/AIAA Spaceflight Mechanics Meeting, San Diego, California, February 2010.
[8] Guzzetti, D., E. M. Zimovan, K. C. Howell, and D. C. Davis, "Stationkeeping Methodologies for Spacecraft in Lunar Near Rectilinear Halo Orbits," AAS/AIAA Spaceflight Mechanics Meeting, San Antonio, Texas, February 2017.
[9] Folta, D., M. Woodard, and D. Cosgrove, "Stationkeeping of the First Earth-Moon Libration Orbiters: the ARTEMIS Mission," AAS/AIAA Astrodynamics Specialists Meeting, Girdwood, AK, August 2011.
[10] Folta, D. C., T. A. Pavlak, A. F. Haapala, and K. C. Howell, Preliminary Design Considerations for Access and Operations in Earth-Moon L_1/L_2 Orbits," AAS/AIAA Spaceflight Mechanics Meeting, Kauai, Hawaii, February 2013.
[11] Petersen, J. and J. Brown, "Applying Dynamical Systems Theory to Optimize Libration Point Orbit Stationkeeping Maneuvers for WIND," AAS/AIAA Astrodynamics Specialists Conference, San Diego, California, August 2014.
[12] D. Folta, T. Pavlak, A. Haapala, K. Howell, and M. Woodard, "Earth–Moon libration point orbit stationkeeping: theory, modeling, and operations," Acta Astronautica, Vol. 94, No. 1, 2014, pp. 421–433.
[13] Davis, D. C., S. A Bhatt, K. C. Howell, J. Jang, R. L. Whitley, F. D. Clark, D. Guzzetti, E. M. Zimovan, and G. H. Barton, "Orbit Maintenance and Navigation of Human Spacecraft in Cislunar Near Rectilinear Halo Orbits," AAS/AIAA Spaceflight Mechanics Meeting, San Antonio, Texas, February 2017.
[14] M. Lo and S. Ross, ''Low energy interplanetary transfers using invariant manifolds of L1, L2 and halo orbits,'' AAS/AIAA Space Flight Mechanics Meeting, Monterey, California, February 1998.
[15] Gomez, G., W. S. Koon, M. W. Lo, J. E. Marsden, J. Masdemont, and S. D. Ross, "Connecting orbits and invariant manifolds in the spatial restricted three-body problem," Nonlinearity, Vol. 17, No. 5, May 2004.
[16] Howell, K., and M. Kakoi, "Transfers between the Earth-Moon and Sun-Earth Systems using Manifolds and Transit Orbits," Acta Astronautica, Vol. 59, 2006, pp. 367-380.
[17] Villac, B. F. and D. J. Scheeres, "Escaping Trajectories in the Hill Three-Body Problem and Applications," *Journal of Guidance, Control, and Dynamics*, Vol. 26, No. 2, March-April 2003.
[18] Davis, D. C. and K. C. Howell, "Characterization of Trajectories Near the Smaller Primary in the Restricted Problem for Applications," *Journal of Guidance, Control, and Dynamics*, Vol. 35, No. 1, January-February 2012.
[19] Grebow, D. "Generating Periodic Orbits in the Circular Restricted Three-Body Problem with Applications to Lunar South Pole Coverage," M.S., May 2006.
[20] J. Breakwell and J. Brown, "The 'Halo' Family of 3-Dimensional Periodic Orbits in the Earth-Moon Restricted 3-Body Problem," Celestial Mechanics, Vol. 20, November 1979.
[21] K. Howell and J. Breakwell, "Almost Rectilinear Halo Orbits," 20th Aerospace Sciences Meeting, 1982.
[22] Grebow, D., D. Ozimek, K. Howell, and D. Folta, "Multibody Orbit Architectures for Lunar South Pole Coverage," Journal of Spacecraft and Rockets, Vol. 45, March 2008.
[23] I. Robin and V. Markellos, "Numerical Determinations of three-dimensional orbits generated from vertical selfresonant satellite orbits." Celestial Mechanics, Nov. 21, May 1980, pp. 395-434.
[24] Zimovan, E., K. C. Howell, and D. C. Davis, "Near Rectilinear Halo Orbits and Their Application in Cis-Lunar Space," 3rd IAA Conference on Dynamics and Control of Space Systems, Moscow, Russia, May-June 2017.
[25] Davis, D. C., S. M. Phillips, and B. P. McCarthy, "Multi-body Mission Design using the Deep Space Trajectory Explorer," AAS/AIAA Spaceflight Mechanics Meeting, Napa, California, February 2016.
[26] Haapala, A. and K. C. Howell, "Representations of Higher-Dimensional Poincaré Maps with Application to Spacecraft Trajectory Design," IAF 63rd International Astronautical Congress, Naples, Italy, October 2012.
[27] Haapala, A., and Howell, K.C., "A Framework for Construction of Transfers Linking Periodic Libration Point Orbits in the Earth-Moon Spatial Circular Restricted Three-Body Problem," *Journal of Bifurcations and Chaos*, Vol. 26, No. 5, May 2016.
[28] Davis, D. C., S. M. Phillips, and B. P. McCarthy, "Trajectory Design for Saturnian Ocean Worlds Orbiters using Multidimensional Poincaré Maps," 67th International Astronautical Congress, Guadalajara, Mexico, September 2016.
[29] Ocampo, C., "Cislunar Orbit Transfer Studies," Presentation to the Future Capabilties Trajectory Team, February 24, 2017.
[30] McGuire, M., L., L. M. Burke, S. L. McCarty, K. J. Hack, R. J. Whitley, D. C. Davis, and C. Ocampo, "Low Thrust Cis-Lunar Transfers using a 40 kW-Class Solar Electric Propulsion Spacecraft," AAS/AIAA Astrodynamics Specialists Conference, Stevenson, Washington, August 2017.